

ISCI, Volume 7

Supplemental Information

Millimeter-Scale Nonlocal Photo-Sensing

Based on Single-Crystal

Perovskite Photodetector

Yu-Tao Li, Guang-Yang Gou, Lin-Sen Li, He Tian, Xin Cong, Zhen-Yi Ju, Ye Tian, Xiang-Shun Geng, Ping-Heng Tan, Yi Yang, and Tian-Ling Ren

1. Transparent Methods

Synthesis of Perovskite single crystals: The MAPbBr₃ single crystals were synthesized via an anti-solvent method with slight modification (Shi et al., 2015). In briefly, 0.734 g PbBr₂ and 0.269 g CH₃NH₃Br were dissolved in 2 mL N, N-dimethylformamide (DMF). Subsequently, 2 mL CH₂Cl₂ as anti-solvent was diffused into perovskite solution slowly, and then small single crystals (~1-2 mm in size) precipitate out. For large crystal growth, by placing the small crystal into fresh solution and repeating the above process, larger crystal (~ 4 mm) was formed.

Fabrication of position-dependent photodetector: Perovskite single crystals (MAPbBr₃) was synthesized through solution process. Then hard mask with defined patterning was covered on the surface of the MAPbBr₃ and fixed by the polyimide tape. Finally, 50 nm Au electrodes were made by conventional electron beam evaporation to define shaped source and drain with a channel of 150 μm width and 120 μm length.

Performance measurement of the position-dependent photodetector: A custom-designed photoelectric measuring system was built by assembling three instruments: the Raman spectrometer, portable probe station, and KEITHLEY 2614B SourceMeter. A focused laser beam with the wavelength of 553 nm (spot size~5 μm) was introduced as the excitation sources, which moved in a direction perpendicular to the perovskite channel. The laser intensity was adjusted by the optical attenuator in the Raman spectrometer and was tested at the objective of the microscope before photodetection properties characterization. Two probes were connected to the Au electrodes to detect the signal. The current signal was recorded using KEITHLEY 2614B SourceMeter.

2.

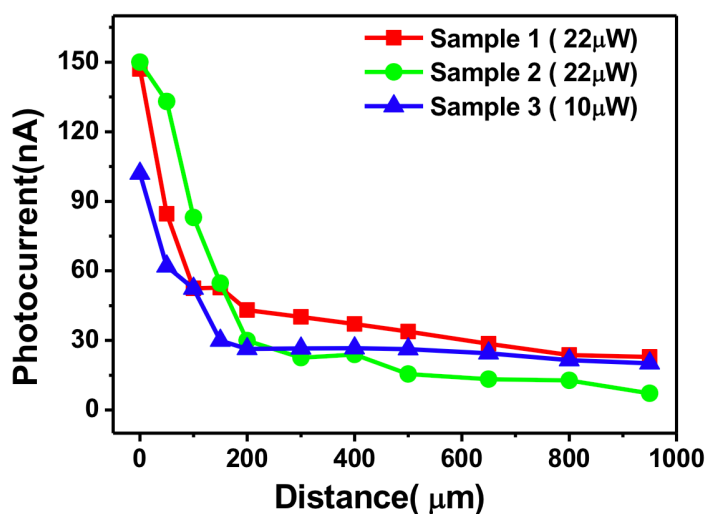


Figure S1. Photocurrents of the three samples as a function of distance at voltage bias of 10 V, related to Figure 3. The results proof the repeatability of the experiment is well. The devices were tested under the laser of 553 nm with laser power of 22 μW (Sample 1, 2) and 10 μW (Sample 3).

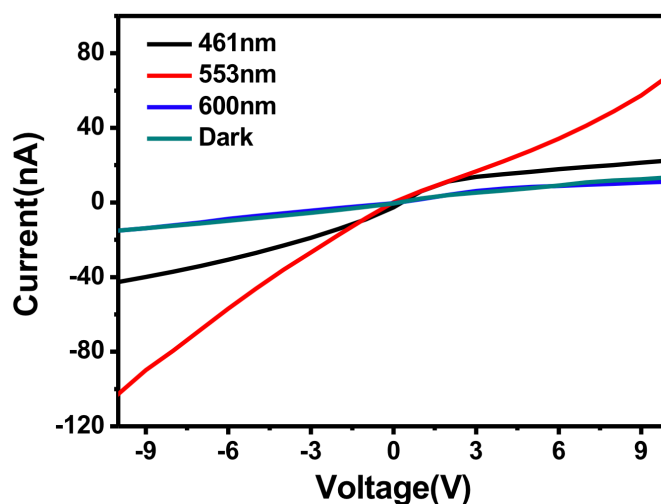


Figure S2. The photoresponse of sample 3 under different wavelengths of the light illumination (10 μW), related to Figure 2. The light current of the device increases with the wavelength approaching 553nm. When it reaches 600nm, the light current is almost the same as the dark current.

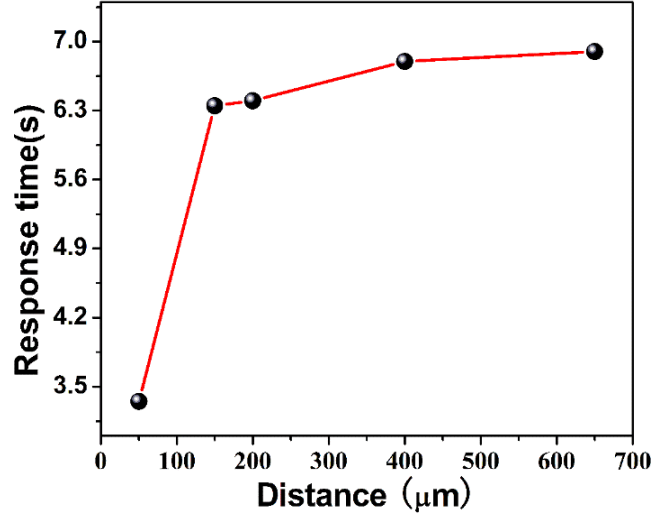


Figure S3. The corresponding raise time of the perovskite device (Sample 1), related to Figure 3. The raise time increases from 3.5 to 6.9 s as the focused distance gradually increased under illumination of 22 μW , which shows the opposite tendency compared to the photocurrent.

3. Calculation of carrier diffusion length

The diffusion length of the MAPbBr_3 single crystal can be determined by the following formula:

$$L_D = \left(\frac{k_B T \mu \tau_r}{e} \right)^{\frac{1}{2}} \quad (\text{S1})$$

where k_B , T , μ and e are the Boltzmann constant, absolute temperature, carrier mobilities, and elementary charge, respectively. τ_r is the carrier lifetime which can be acquired from time-resolved photoluminescence. (Shown in Figure 3e).

According to Mott-Gurney law, a trap-filling process is identified by the marked increase of the current injection at a bias range higher than 10 V in Figure S4, and the device dark current (J_D) is measured to derive carrier mobilities:

$$J_D = \frac{9 \epsilon \epsilon_0 \mu V_b^2}{8 L^3} \quad (\text{S2})$$

where L is the distance between the center of the two Au pads, ϵ ($= 32$) is the relative dielectric constant of MAPbBr₃, and ϵ_0 is the vacuum permittivity. V_b is the applied voltage. Large hole mobility of $51.3 \text{ cm}^2 \text{ S}^{-1} \text{ V}^{-1}$ is derived from the curve fitting. Hence, the diffusion length calculated from the two formulas is $7.3 \text{ }\mu\text{m}$, which matches the previous report well (Saidaminov et al., 2015). Besides, According to the operation instructions (version 3.4.0) of EDINBURGH PHOTONICS company, the fitting curve of time-resolved photoluminescence of MAPbBr₃ single crystal under different laser intensity was acquired, Thus, we can get the fitting carrier lifetimes and the diffusion lengths under different laser intensities in Figure 3f from above methods.

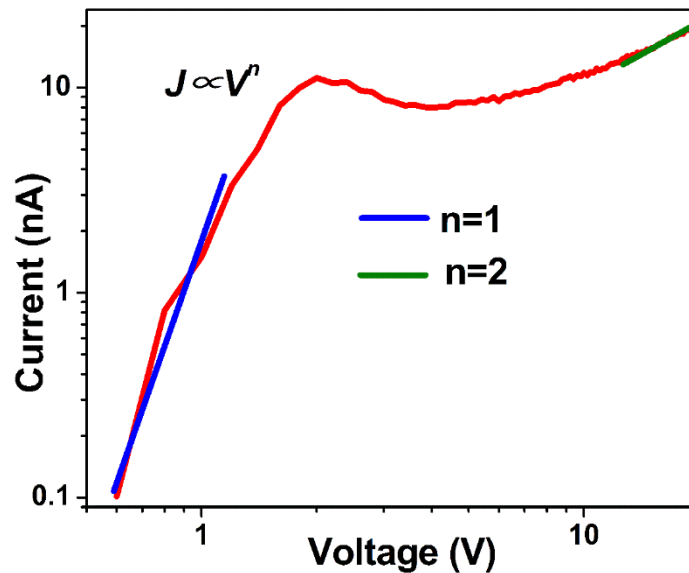


Figure S4. The dark current-voltage curve for a MAPbBr₃ device, related to **Figure 3**. The result is well fitted (green line) by the Mott-Gurney law (Dong et al., 2015).

4. Nonlocal photo-response measured and model simulation

The simulation suggests that our model can explain the observed position dependent photo-response experimental data quite well. Here we provide an in-depth discussion of our model organization. The flowchart of our model simulation is shown as followed:

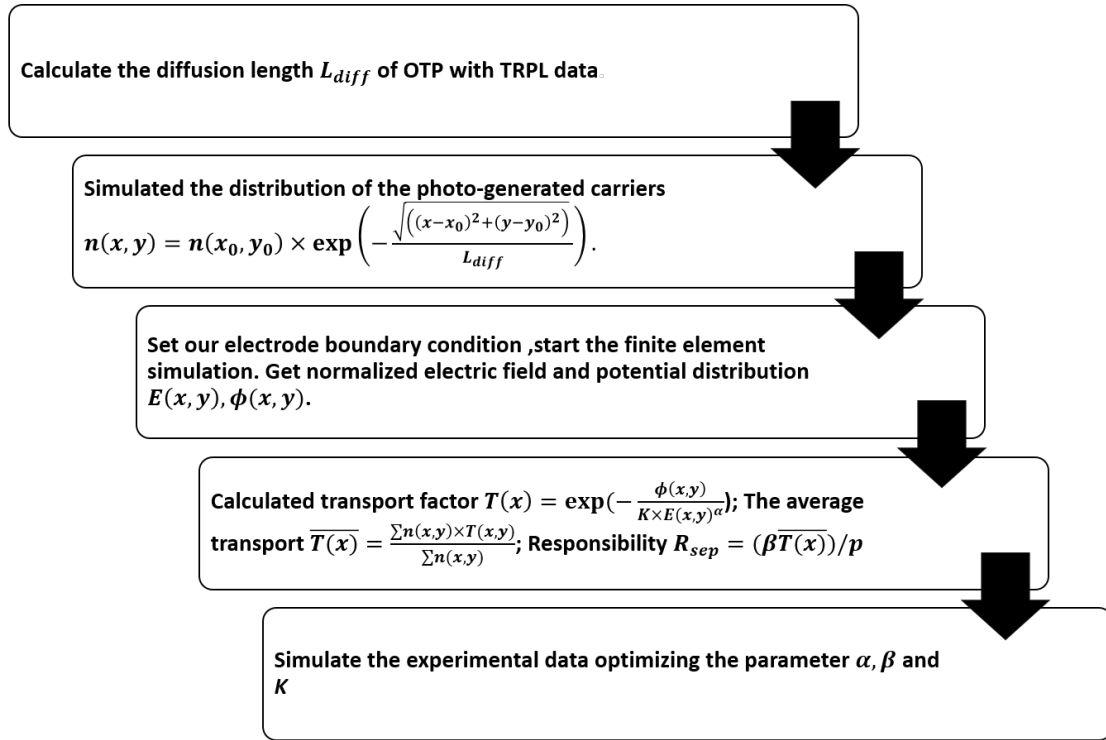


Figure S5. The flowchart of our model simulation, related to Figure 4. The flowchart describes the five steps of the device performance simulation.

The average transport factor is calculated considering the initial diffusion carriers before applying the electric field. Within the circle with radius of $r_{max} = 50 \mu\text{m}$, we consider the initial photo-generated distribution as an exponential damping $n(x, y) = n(x_0, y_0) \times \exp\left(-\frac{\sqrt{(x-x_0)^2 + (y-y_0)^2}}{L_{diff}}\right)$. Here, x_0 and y_0 are coordinate of the circle center where the laser spots on. L_{diff} is the diffusion length of the MAPbBr₃ single crystal, calculated in the main text. So, we can calculate the average transport factor $T(x)_{avg} = \frac{\sum_{r < r_{max}} n(x, y) \times T(x, y)}{\sum_{r < r_{max}} n(x, y)}$. To simplify our simulation, we can normalize the average transport factor $\overline{T(x)}_0$ with $\overline{T(0)}_0$ (the average transport factor at $x = 0 \mu\text{m}$), where the photo-generated current is the largest. Consequently, there is the normalization average transport factor $\overline{T(x)} = \frac{T(x)_{avg}}{T(0)_{avg}}$ in our model. But the distribution of $T(x, y)$ is still needed in our model for $T(x)_{avg}$ calculation (Sarker et al., 2017).

$$T(x, y) = \exp\left(-\frac{d_{total}}{L_{eff}}\right) = \exp\left(-\int_0^\varphi \frac{d\varphi}{EL_{eff}}\right) \quad (S3)$$

$$\frac{1}{L_{eff}} = \frac{1}{L_1} + \frac{1}{L_2} \quad (S4)$$

where E and φ are the electric field and electric potential along the direction of the electric field line. There are two characteristic scale lengths in a general problem, L_1 and L_2 . They both exhibit a mixture of drift and diffusion. For high electric field values, L_1 is reduced as E^{-1} , while the absolute value of L_2 increases as E , which both exhibit a mixture of drift and diffusion (Del Alamo, 2009). Hence, we can also introduce an experimental ideality factor $0 < \alpha < 2$ in our model combining the effect of diffusion and recombination. Such parameter α will also include the nonlinearity introduced by the non-uniform electrical field. Consequently, we can simplify the contribution of different carriers as shown in the main text by the following formulas:

$$\frac{1}{EL_{eff}} = C1 \times \left(\frac{E}{E_0}\right)^0 + C2 \times \left(\frac{E}{E_0}\right)^{-2} = C \times E(x, y)^{-\alpha} \quad (S5)$$

$$T(x, y) = \exp\left(-\frac{\varphi(x, y)}{K \times E(x, y)^\alpha}\right); \quad \varphi(x, y) = \frac{\varphi}{\varphi_0} \quad (S6)$$

where the normalization constants ($E_0 = 1 \text{ V/m}$, $\varphi_0 = 1 \text{ V}$) are used to simplify the calculation by changing the electric field to the absolute value. $\varphi(x, y)$ is the normalization electric potential value (the relative electric potential value compared to the potential of 1V) at the position that carriers generated; $E(x, y)$ is the normalization electric field value (the relative electric field value compared to the potential of 1V/m) at the position the same as $\varphi(x, y)$. K is a normalization parameter in this model.

As the α is close to 0, L_1 has more contribution on the L_{eff} . L_1 is considered as generalized diffusion length, the mean distance that the carrier diffuses in the bulk of a semiconductor. Consequently, if the α is close to 0 when fitting on the experimental data, the diffusion process will have much greater contribution than the recombination process during the carriers transport in such materials. The simulated results for different α are also shown as followed. As the distance increases, we can observe that the photocurrent generated will have a quicker drop when the α is closer

to 0. We can fit the experimental data to get such parameter α to determine the contribution of the diffusion and the recombination during the transport.

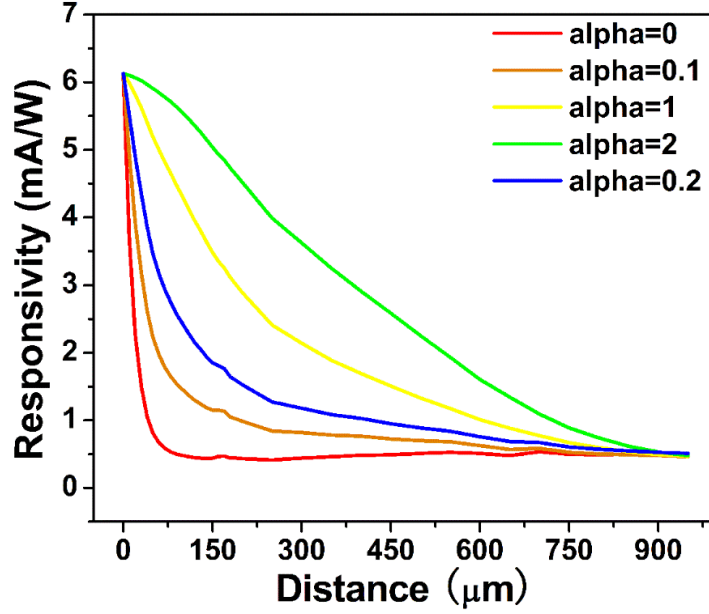


Figure S6. The simulated responsivities for different α parameters, related to **Figure 4**. The generated photocurrent will have a quicker drop when the α is closer to zero.

After fitting the experimental data with different incident laser intensities, it can be observed that the parameter α should become smaller to fit the curve with lower incident laser power, which means that the diffusion process has much more contribution than the recombination process when the incident power decreases. It can be attributed to the lower net recombination rate, which indicates that the recombination process has less contribution than the situation with high power incident laser. Since the net recombination rates are proportional to the excess np carriers product due to the band-to-band optical process, which is lower as the incident power decreased. As a result, we are expected to apply smaller α parameter to fit our experimental data well as the incident laser declined.

$$I_{\text{photo}}(x) = \beta(p)\overline{T(x)} \quad (S7)$$

For the photocurrent simulation formulas, the $\beta(p)$ is the current generated factor related to the incident laser power p . The nonlinearity photocurrents generation of the MAPbBr₃ at $x=0$ μm under different incident laser powers are shown in Figure 2(b) in the main text. In our calculation, we take the photocurrents generated at $x = 0$ μm as our current generated factor $\beta(p)$. $\overline{T(x)}$ is the normalization average transport factor which will be one at $x = 0$ μm . Consequently, our model can calculate the photocurrents in different locations and our results are good.

Thus the simulation parameters $\{\alpha, K, \beta(p)\}$ are $\{0.1, 0.23, 53.3 \text{ nA}\}$, $\{0.15, 0.165, 99.5 \text{ nA}\}$ and $\{0.2, 0.14, 135 \text{ nA}\}$ for different incident light intensities at 3.55, 9.7 and 22 μW , respectively. The simulation results are shown in the Figure 4c in the main text.

Supplemental References

Del Alamo, J.A. (2009) *Integrated Microelectronic Devices: Physics and Modeling*. (Pearson Education).

Dong, Q., Fang, Y., Shao, Y., Mulligan, P., Qiu, J., Cao, L., and Huang, J. (2015). Electron-hole diffusion lengths >175 μm in solution-grown CH₃NH₃PbI₃ single crystals. *Science* 347, 967–970.

Saidaminov, M.I., Adinolfi, V., Comin, R., Abdelhady, A.L., Peng, W., Dursun, I., Yuan, M., Hoogland, S., Sargent, E.H., and Bakr, O.M. (2015). Planar-integrated single-crystalline perovskite photodetectors. *Nat. Commun.* 6, 8724.

Sarker, B.K., Cazalas, E., Chung, T.-F., Childres, I., Jovanovic, I., and Chen, Y.P. (2017). Position-dependent and millimetre-range photodetection in phototransistors with micrometre-scale graphene on SiC. *Nature. Nanotech.* 12, 668.

Shi, D., Adinolfi, V., Comin, R., Yuan, M., Alarousu, E., Buin, A., Chen, Y., Hoogland, S., Rothenberger, A., and Katsiev, K. (2015). Low trap-state density and long carrier diffusion in organolead trihalide perovskite single crystals. *Science* 347, 519–522.